# Photovoltaic spatial light modulator

John H. Hong, Frederick Vachss, Scott Campbell, and Pochi Yeh
*Rockwell Science Center, 1049 Camino dos Rios, Thousand Oaks, California 91360*

(Received 3 August 1990; accepted for publication 21 November 1990)

A novel concept for implementing a high-resolution spatial light modulator using a thin slab of photorefractive $LiNbO_3$ crystal is described. This method uses the photovoltaic effect to impress phase information onto the crystal without the use of holography where coherent reference beams are required. Experimental demonstration as well as an analysis of the operation and performance of the device are given.

## I. INTRODUCTION

A basic need in most optical information-processing systems is the interfacing requirement, i.e., the need to provide input to and extract output from the optical system. Generally speaking, the input function is performed by devices called spatial light modulators (SLM). Such a device imposes a given set of information on an optical wave by spatially modulating its intensity and/or phase distribution. An optical processor then operates on the spatially modulated optical beam to yield some desired computational result, which is extracted by an appropriate output device such as a detector. Optical correlation systems,[1] optical vector matrix multipliers,[2] and, more recently, optical neural networks[3] are examples in which the SLM is a necessary component.

Photorefractive holography has already been used successfully to implement an optically addressed SLM, the so-called "photorefractive incoherent-to-coherent optical converter"[4,5] (PICOC) (Fig. 1). First, a dynamic holographic grating is created inside a photorefractive slab with two coherent plane waves. An incoherent object is then imaged onto the crystal; the incoherent image partially erases portions of the dynamic grating, which is continuously supported by the two writing beams. The partially erased grating is then read out with a reading beam whose diffracted component contains the spatial modulation imposed by the erasing incoherent image. High resolution (upwards of 15 lp/mm) has been achieved with this method. Because the system is inherently holographic, however, it is subject to tight alignment as well as vibrational requirements.

Information (i.e., images) can be imprinted in photorefractive crystals without resorting to holographic techniques as shown in Fig. 2 where an incoherent intensity pattern is imaged onto a photorefractive crystal across which a large electric field is imposed. The nonuniform illumination causes local variations in the conductivity of the crystal (via photoconductivity), resulting in nonuniform screening of the electric field. The spatially varying electric field induces index perturbations via the electro-optic effect; the index perturbations are read out using coherent light, either as a phase image or, by using crossed polarizers, as an intensity image. This technique has been demonstrated by Yu[6] for $Bi_{12}SiO_{20}$ and also by Steir, Kumar, and Ziari for CdTe.[7] Such methods, however, require large external voltages and are difficult to generalize for two-dimensional spatial light modulation.

## II. PHOTOVOLTAIC PHASE MODULATION

Our technique[8] achieves similar results without the need for external voltages by utilizing the bulk photovoltaic effect exhibited by certain ferroelectric crystals such as lithium niobate ($LiNbO_3$). The photovoltaic effect is characterized by a photocurrent in the absence of an external field, distinguishing it from photoconductivity. It is widely accepted that the origin of the effect is due to asymmetric charge transfer during photoexcitation.[9] If such a crystal is flooded uniformly with light, then a short-circuit current can be measured (or, equivalently, an open-circuit voltage) across the crystal. If, however, as illustrated in Fig. 3, the crystal is exposed to a nonuniform distribution of light, in this case in the form of a rectangular window function, then charges accumulate at the light-dark boundaries within the crystal. The associated space-charge field modulates the index of refraction via the electro-optic effect, resulting in a nonuniform spatial phase distribution as seen by a coherent read beam passing through the crystal. This is the principle of operation of the spatial light modulation scheme. By simply imaging an incoherent object onto the photovoltaic crystal, information in the form of phase modulation is recorded, which is then read out with a coherent reading beam.

## III. EXPERIMENTS AND DISCUSSION

In our experiments, we used a 1-mm-thick, Fe-doped (0.08%) $LiNbO_3$ as the photovoltaic material with the broad faces parallel to the $xz$ plane of the crystal. The image recorded in such a crystal is expected to accentuate features that vary along the $c$ axis due to the anisotropy of both the photovoltaic and electro-optic effects. The basic recording/reading experiment is shown in Fig. 4 where $\lambda = 514.5$

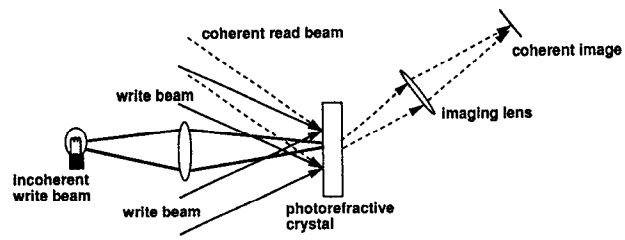


FIG. 1. Photorefractive incoherent-to-coherent optical converter (PICOC).

 0021-8979/91/052835-06$03.00  

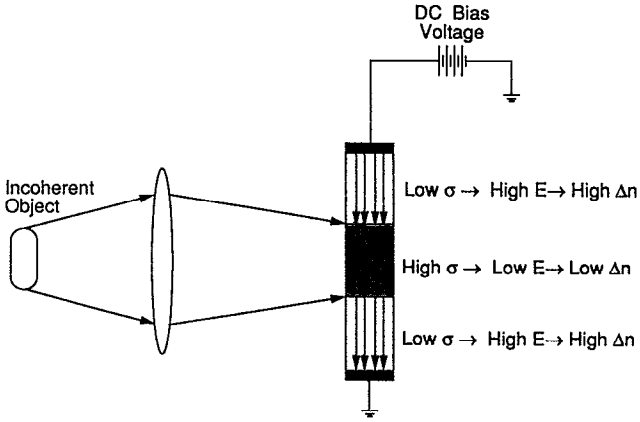


FIG. 2. Nonholographic image recording using photoconductivity.

nm light from an argon-ion laser supplies both writing and reading beams. The writing beam (ordinary polarization) intensity was 8 mW/cm$^2$, and the reading beam (extraordinary polarization) was 400 $\mu$W/cm$^2$. The choices of the beam polarizations were dictated by the electro-optic coefficients. The writing beam should "see" as small an index perturbation as possible during the writing process so as to reduce self-defocusing (ordinary beam "sees" $r_{13}$, which is a factor of 3 smaller than $r_{33}$, which is "seen" by the reading beam). Various images (Ronchi rulings and Air Force resolution chart) with spatial detail ranging from $\sim 10\,\mu$m to grosser scale structures (1 mm and greater) were used. Since the spatial modulation is phase-only, the modulated beam had to be either defocused or spatially filtered (in the Fourier plane) to be visualized. The results thus obtained are summarized in Fig. 5 where the anisotropy of the spatial phase modulation due to the tensor nature of both photovoltaic and electro-optic effects is striking. At the intensity levels used, about 15 min were taken to write the images to saturation. Note that, as in the photorefractive effect, this factor can be reduced substantially by increasing the intensity level.

To rigorously analyze the SLM response, we need to resort to a system of nonlinear equations governing the generation, recombination, and transport of charged carriers in the photorefractive crystal. In steady state, the equations are[10]

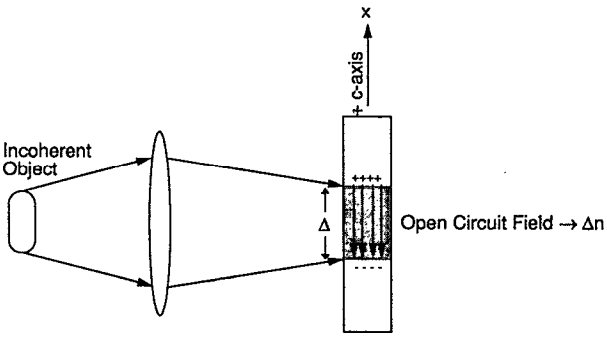


FIG. 3. Nonholographic image recording using photovoltaic effect.

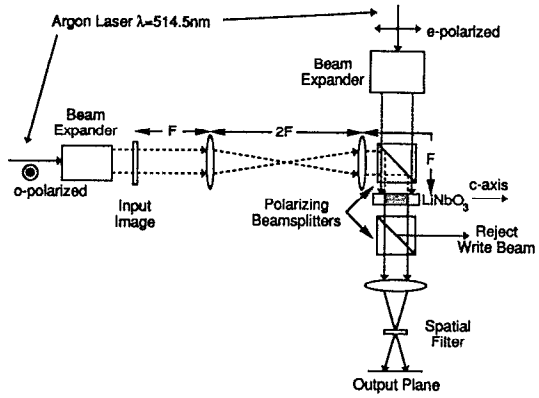


FIG. 4. Experimental system for spatial light modulation using $LiNbO_3$.

$$(sI+\beta)(N_D - N_D^+) = \gamma_R n N_D^+, \tag{1}$$

$$J = en\mu E + k_B T\mu \frac{dn}{dx} - pI, \tag{2}$$

$$\frac{dE}{dx} = \frac{e}{\epsilon}(N_D^+ - n - N_A), \tag{3}$$

where $E$ = electric field, $I$ = incident writing intensity distribution, $J$ = current density, $s$ = ionization cross section, $\beta$ = rate of thermal generation of carriers, $k_B$ = Boltzmann constant, $\mu$ = carrier mobility, $\gamma_R$ = carrier recombination rate, $N_D$ = total density of donors, $N_D^+$ = density of ionized donors, $N_A$ = density of compensating charge for ionized donors, $n$ = density of electrons in the conduction band, $e$ = electronic charge, $\epsilon$ = dielectric constant of crystal, and $p$ = photovoltaic constant. The $x$ axis is defined to be opposite in direction to the $+c$ axis so that the photovoltaic current term in Eq. (2) may differ from other formulations by a sign; the physics is unchanged.

Since the ends of the crystal are left open, $J$ must be zero at those boundaries and hence zero everywhere, in steady-state conditions. To obtain approximate results appropriate for our experiments, we assume linear generation and recombination and neglect Poisson's equation (3), which describes the feedback effect of the charged carriers on the electric field. We are left with the carrier transport equation given by Eq. (2) equated to zero because of the boundary conditions and a linear expression for the carrier density. Further, we neglect the diffusion component of the current density which is the second term in Eq. (2).

With these approximations, we have

$$n(x) = \frac{[sI(x)+\beta](N - N_A)}{\gamma_R N_A}, \tag{4}$$

$$en(x)\mu E(x) - pI(x) = 0. \tag{5}$$

If we assume the specific intensity distribution $I(x) = I_0\,\mathrm{rect}[x/\Delta]$ ($\mathrm{rect}[x] = 1$ if $|x| < 1$; otherwise, $\mathrm{rect}[x] = 0$) as shown in Fig. 3 where $sI_0 \gg \beta$, then the electric-field strength can be determined to be

$$E(x) = \frac{p\gamma_R N_A}{\mu e s(N_D - N_A)}\,\mathrm{rect}[x/\Delta]. \tag{6}$$

In the Appendix, by investigating the complete set of nonlin-

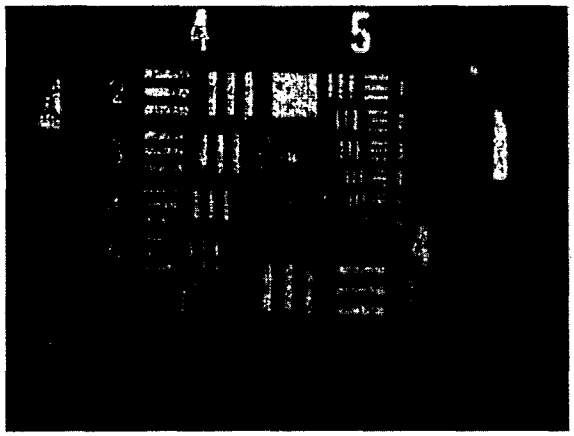


(a)

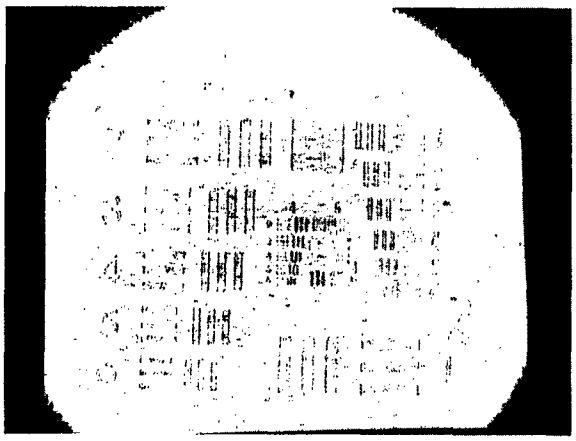

(b)

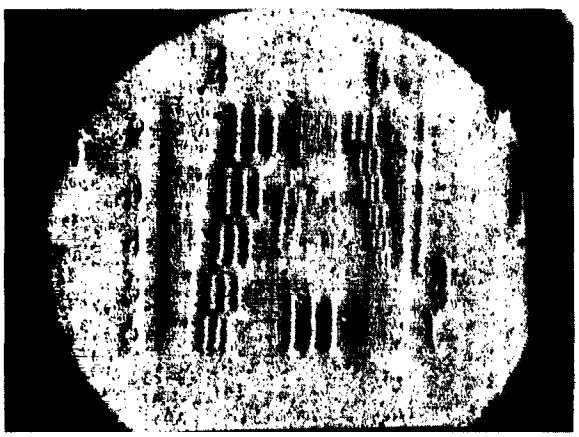

(c)

FIG. 5. Air Force resolution chart imaging results: (a) defocused phase image, (b) spatially filtered image, and (c) image of test chart as seen through the crystal.

ear equations (1)–(3) both analytically and numerically, we show that the actual field deviates minimally from this approximate solution. In particular, the analysis shows that, due to charge saturation and diffusion, the boundaries defined by the borders between the high- and low-intensity illuminated regions become smoothed with narrow transition regions ( $<1\ \mu$m wide). With reference to Fig. 3, the carriers (electrons) generated in the illuminated region are transported away from the $+c$ axis by the photovoltaic effect,[9] resulting in a net positive current flow toward the $+c$ axis. In steady state, charge walls build up at the light-to-dark boundaries, which counterbalance the photovoltaic current to yield a net zero current. The resulting field $E(x)$ then modulates the index of refraction that extraordinary polarized light sees in the crystal. Note that for $sI_0 \gg \beta$, the steady-state electric-field strength is independent of intensity. The index change in the given orientation is

$$\Delta n(x) = -\frac{n_e^3 r_{33}}{2} E(x)$$

$$= -\frac{n_e^3 r_{33}}{2} \frac{p\gamma_R N_A}{\mu es(N_D - N_A)} \operatorname{rect}[x/\Delta]. \quad (7)$$

This index change was experimentally measured using a Mach–Zehnder interferometer. A collimated writing beam ($\lambda_w = 514.5$ nm, $I = 8$ mW/cm$^2$, ordinary polarized) from an argon laser is passed through a square opening (0.25 cm$\times$0.25 cm), which is imaged onto the $LiNbO_3$ crystal, while a collimated extraordinary polarized beam from the same laser ($I = 400\,\mu$W/cm$^2$) was used as the source for the interferometer, in one leg of which the crystal was placed. In this way, the index change could be measured by careful observation of the output fringe pattern. The interferogram thus obtained is shown in Fig. 6. Note the steplike change in the fringe pattern shown in Fig. 6 corresponding to the dark-light and light-dark boundaries. Denoting the index change in the illuminated region by $\Delta n_0$, the total optical phase shift is given by $\Delta\phi/2\pi = \Delta n_0\, d/\lambda$, where $d = 1$ mm, the thickness of the crystal. Using an estimate for the observed fringe shift in the illuminated region of about 90°, the index change can be calculated to yield $\Delta n_0 \approx 1.29\times 10^{-4}$.

According to Eq. (7), the saturation value of the index change is proportional to the empty trap concentration. Thus, an oxidized $LiNbO_3$ crystal (high $Fe^{3+}$ concentration) will yield larger index changes. For resolution considerations, it is desirable to have a thin crystal which requires high trap concentration.

One final device parameter to be discussed is the response time. Although the response time we obtained was on the order of minutes, it can be decreased considerably by altering the dopant concentration. The response time is the standard photorefractive time constant given by[10]

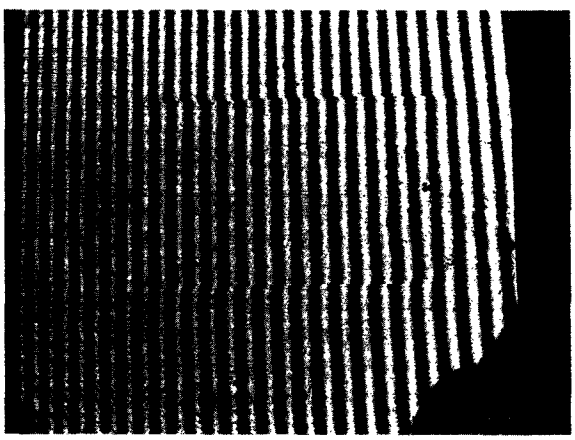

FIG. 6. Interferogram for square image.

$$\tau = \frac{\gamma_R \epsilon N_A}{(N_D - N_A) e\mu s I_0}. \tag{8}$$

By increasing the donor concentration $N_D$ relative to the empty trap concentration, the response time can be reduced. For optimum device performance, $N_D$ must be as high as possible and the oxidation state must be controlled ($N_A$) to give the appropriate index change.

## IV. SUMMARY

In summary, we have demonstrated a phase-only spatial light modulator using a photorefractive crystal in a nonholographic geometry. The discussions given indicate a one-dimensional modulation, which is due to the anisotropy of the $LiNbO_3$ crystal used in our experiments. The concept is easily extended to the more general and useful two-dimensional case by sandwiching two similar crystals whose $c$-axis orientations are orthogonal to one another.

## APPENDIX: DEPENDENCE OF DEVICE RESOLUTION ON MATERIAL PARAMETERS

A practical definition of the limiting resolution of the device is the minimum feature size that can be imposed while some acceptable level of contrast in the output image is maintained. While the exact definition may vary somewhat depending on one's criteria of acceptability, we shall show that certain image length scales exist above which the contrast and replication fidelity are quite good and below which these qualities rapidly degrade. As these length scales are determined by the physics of the recording process, it will be necessary to analyze the charge transport equations underlying this process to determine these scales and the resolution limits they imply.

Examining the steady-state equations (1)–(3), we see that when the input image intensity $I(x)$ is simply a constant: the charge densities $n$ and $N_D^+$ and hence the internal electric field $E$ are also constant. It is thus reasonable to assume that for sufficiently slow variations in $I(x)$, all terms involving the spatial derivatives of $n$, $N_D^+$, and $E$ may be neglected and the response field will still be given by

$$E(x) = \frac{p\gamma_R N_A}{e\mu(N_D - N_A)} \frac{I(x)}{sI(x) + \beta}. \tag{A1}$$

This is the local (albeit nonlinear) photovoltaic response described in Sec. III. When $I(x)$ varies more rapidly, these spatial derivative terms may no longer be ignored and deviations from the local response described in Eq. (A1) occur. These deviations from local response eventually determine the achievable resolution. In the remainder of this appendix, we will analyze solutions to Eqs. (1)–(3), including the derivative terms, and in so doing will describe the behavior of the resultant deviations from local response and their implications on device resolution.

Since Eqs. (1)–(3) form a second-order nonlinear system for which analytic solutions are not generally available, we must restrict our analysis somewhat to obtain useful results. First, we shall make the common assumption[11,12] that the incident intensity is sufficiently weak so that photoconductive saturation does not occur (i.e., $n \ll N_D^+$). We note that this assumption, when applied to Eq. (3), implies that

$$-\frac{e}{\epsilon} N_A < \frac{dE}{dx} < \frac{e}{\epsilon}(N_D - N_A), \tag{A2}$$

since $0 < N_D^+ < N_D$. This restriction on the slope of the space-charge field due to charge saturation effects is one of the factors determining the effective resolution limit.

In addition, we shall only consider input intensities that are piecewise constant in space. This is consistent with the bar pattern intensities used in our experiments and allows us to take $dI/dx = 0$ everywhere except at some isolated collection of points corresponding to the steps in intensity. Since any continuous function may be approximated arbitrarily well by a step function of sufficiently small step size, this assumption of piecewise constancy is not overly restrictive. The fact that we can now ignore the derivatives of $I(x)$ permits us to combine the steady-state charge transport equations into the single, relatively simple second-order nonlinear equation for the internal space-charge field $E(x)$:

$$E(x)\left[\left(1 - \frac{\epsilon}{e(N_D - N_A)} \frac{dE}{dx}\right) \Big/ \left(1 + \frac{\epsilon}{eN_A} \frac{dE}{dx}\right)\right] - \left(\frac{\epsilon k_B T}{e^2 N_A (N_D - N_A)} \frac{d^2E}{dx^2}\right) \Big/ \left(1 + \frac{\epsilon}{eN_A} \frac{dE}{dx}\right)^2 = E_p, \tag{A3}$$

where $E_P$ is the nominal photovoltaic space-charge field as defined in (A1).

Since Eq. (A3) is valid in each of the regions of constant intensity, the effects of the variation in $I(x)$ are now taken into account by requiring that $E(x)$ and its derivative remain continuous across the boundaries at which the intensity changes. Given Eq. (A3) defining $E(x)$, we approach the solution in two steps. First, we may solve this equation directly in the limit of negligible diffusion ($E_D = 0$). The effects of diffusion are then included by applying a simple form of boundary layer analysis to the diffusion-free solution.

In the absence of diffusion effects, Eq. (A3) is reduced to the first-order equation

$$\frac{dE}{dx} = \frac{e}{\epsilon} N_A (N_D - N_A) \frac{E(x) - E_p}{(N_D - N_A)E_p + N_A E(x)}. \tag{A4}$$

While it is straightforward to integrate this equation and obtain an implicit expression for the diffusion-free space-charge field, it is somewhat simpler and equally instructive to observe certain general analytic properties of Eq. (A4). First, we see that for $E(x) \cong E_P$, Eq. (A4) implies that the space-charge field diverges from $E_P$ exponentially according to

$$E(x) \cong E_P + [E(0) - E_P]\exp(x/L_0), \tag{A5a}$$

where

$$L_0 \equiv \frac{\epsilon N_D E_P}{eN_A (N_D - N_A)}. \tag{A5b}$$

We note that this monotonic divergence implies that $E(x)$ must always lie between the maximum and minimum values of $E_P(x)$. In particular, in our sign convention taking the $+c$ axis of the material as the negative $x$ direction, Eq. (A1) implies that $E_P \geqslant 0$. In addition, we see that $E_P$ reaches a

maximum value of

$$E_{\max} \equiv \frac{p\gamma_R}{\mu e s} \frac{N_A}{N_D - N_A}, \tag{A6}$$

when the incident intensity is large enough that photoconductivity substantially exceeds the dark conductivity of the medium. Combining these two results with the requirement that the space-charge field must lie between the extremal values of $E_P$, we obtain the requirement that $0 < E(x) < E_{\max}$. This requirement further implies that the exponential length scale $L_0$ given in Eq. (A5b) takes on a maximum value of

$$L_0(\max) = \frac{\epsilon N_D E_{\max}}{e N_A (N_D - N_A)}, \tag{A7}$$

when $E_P = E_{\max}$. Assuming that the nominal photovoltaic field does indeed stay near $E_{\max}$ (as is usually the case for significant levels of illumination), we thus may use $L_0(\max)$ as an effective minimum resolution scale.

The exponential behavior described in Eq. (A5) persists until $|E(x) - E_P|$ grows sufficiently large that the slope of $E(x)$ approaches the limits given in Eq. (A2). In particular, if $E(x) > E_P$, then as $E(x) - E_P$ grows to near $E_P N_D / N_A$, the exponential growth of Eq. (A5) becomes linear with the maximum slope of $dE/dx \cong e/\epsilon(N_D - N_A)$. Conversely, if $E(x) < E_P$, then as $E(x)$ decreases, the slope also decreases and approaches its minimum value of $dE/dx \cong -eN_A/\epsilon$ as $E(x)$ approaches zero. These two limiting slopes thus provide specific resolution constraints since a minimum length scale of

$$L_{\min} = \left| \Delta E \Big/ \left( \frac{dE}{dx} \right)_{\max} \right| \tag{A8}$$

is required for a change in value of $|\Delta E|$ to be achieved with a maximum slope magnitude $|(dE/dx)_{\max}|$. Specifically, since any changes $\Delta E$ in the space-charge field from region to region must satisfy $|\Delta E| < E_{\max}$, we may combine Eqs. (A6) and (A8) with the slope constraints of Eq. (A2) to obtain the minimum resolution scales:

$$L_{\min} = \epsilon E_{\max}/eN_A, \quad \epsilon E_{\max}/[e(N_D - N_A)]. \tag{A9}$$

Since $0 \leqslant N_A \leqslant N_D$, however, we see that $L_0(\max)$ as given in Eq. (A7) exceeds both values for $L_{\min}$ given in Eq. (A9) above. Thus, as the largest of all the resolution constraints we have found, $L_0(\max)$ may be taken as the minimum resolvable feature size for the diffusion-free system described by Eq. (A4).

The diffusion-free results we have described above do not adequately characterize the response of the system when distance scales become very small. In particular, if $E_{\max}$ as given in Eq. (A6) is sufficiently small, the resolution limit in Eq. (A7) can become very small as well and approach the medium's diffusion length. In this regime, diffusion effects significantly impact the achievable resolution, and the full second-order equation given in Eq. (A3) must be considered.

To approach the full solution, we note that diffusion effects are governed by the second spatial derivative term in Eq. (A3). Thus, diffusive effects should cause the most significant modifications to the behavior of our diffusion-free solution in those regions in which this approximate solution exhibits a rapid change in slope. To determine where such rapid changes occur, we recall that the solutions to Eq. (A4) tend to diverge from $E_P$ in a roughly exponential fashion within a given region of constant intensity. This divergence is followed by an abrupt return to near-zero slope as the next illumination boundary is reached and the exponential divergence is repeated in the ensuing constant intensity region.

This behavior is illustrated in Fig. 7(a). Here, an exact solution $E(x)$ to Eq. (A4) is plotted assuming a periodic intensity step pattern. The corresponding step pattern representing the nominal photovoltaic field $E_P(x)$ is shown as dotted lines in the background. Using a value of $N_A/N_D = 0.5$ and choosing the remaining parameters so that $L_0(\max)$ is roughly 0.10 times the thickness of the regions of constant illumination, we find that the quasiexponential behavior described in the preceding paragraphs is indeed present. Most significant though, in the present discussion, is the observation that the slope does in fact change abruptly at the illumination boundaries. We may thus expect the effects of diffusion to be manifested in the formation of boundary layers in the regions of these abrupt transitions. Such boundary layer formation is common[13] in such systems as Eq. (A3) in which a first-order equation is modified by the addition of a small higher-order term.

The evaluation of the behavior of the solution in these boundary regions is simplified by noting that the extrema of $E(x)$ determined from the diffusion-free equation occur at or near these boundaries. It is thus reasonable to determine the solution to Eq. (A3) in the regions of its extrema and to attempt to use these solutions to describe the behavior of the solution at the boundary layers. Specifically, near the extrema of $E(x)$, we may take $dE/dx \cong 0$, and Eq. (A3) simplifies to the linear second-order equation

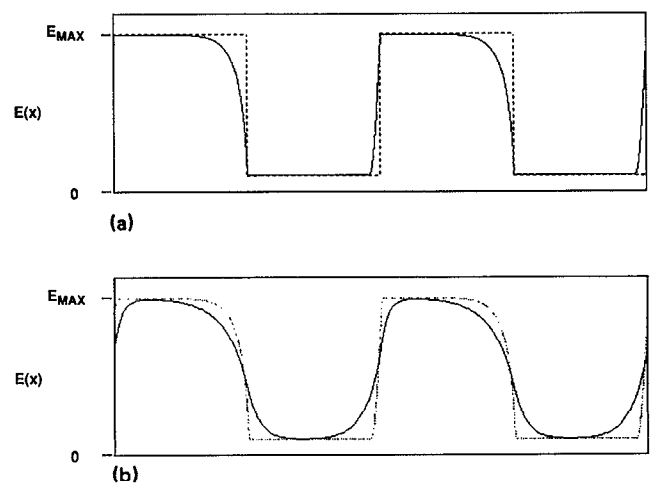


FIG. 7. (a) The exact numerical solution to (A4), $E(x)$ is plotted against position in solid lines. The zeroth-order step-function solution, $E(x) = E_p(x)$, is shown as dashed lines. Note the saturation with constant slope near the illumination boundaries. (b) The exact numerical solution to (A3) is plotted vs position in solid lines along with the solution of Eq. (A4) as dotted lines. Note the replacement of the slope discontinuities of the diffusion-free solution of Eq. (A4) with the smooth extremal behavior of the full second-order result.

$$\frac{d^2E}{dx^2} = \frac{e^2 N_A (1 - N_A/N_D)}{\epsilon k_B T} [E(x) - E_P], \qquad \text{(A10)}$$

which has the solution

$$E(x) = (E_0 - E_P)\cosh[(x - x_0)/L_D], \qquad \text{(A11a)}$$

in the region of the extremum, $E(x_0) = E_0$, where $x_0$ is the location of the maximum (or minimum) of $E(x)$, and

$$L_D \equiv \sqrt{\epsilon k_B T / e^2 N_A (1 - N_A/N_D)} \qquad \text{(A11b)}$$

is the Debye screening length in the medium. We thus expect that instead of the abrupt slope transitions at the illumination boundaries seen in Fig. 7(a), smooth transition regions with widths on the order of $L_D$ will occur. Thus, the Debye screening length provides a second effective minimum resolution scale for our device.

This smooth "coshlike" behavior at the extrema described by Eq. (A11a) will persist until $dE/dx$ grows to the order of $E_P/L_0(\max)$ at which point the solution follows the first-order behavior of the solutions to Eq. (A4). In other words, the exact solution to Eq. (A3) shares the gross features of the earlier solution to Eq. (A4) except for the existence of boundary layers of width $\sim L_D$ near the extrema. This behavior is shown in Fig. 7(b) in which the exact solution to Eq. (A3) is plotted for the same parameter set as was used in Fig. 7(a). Here, in addition, a Debye screening length equal to $L_0(\max)$ is used. The corresponding solution from Fig. 7(a) is shown as dashed lines for comparison. We see from these plots that, as claimed, the two curves share the same general behavior with diffusion effects introducing substantial smoothing in the region of the extrema.

The final result of our analysis is that there are two fundamental resolution limits on the photovoltaic photorefractive device, one imposed by charge saturation limits and the other by charge diffusion effects. Using typical parameters for $LiNbO_3$, we may evaluate these limits and obtain $L_0(\max) \approx L_D \sim 0.5\ \mu$m. Thus, the resolution, as dictated by the physics of the photorefractive/photovoltaic process, is limited to about 1 $\mu$m.


[1] J. W. Goodman, *Introduction to Fourier Optics* (McGraw-Hill, New York, 1968).
[2] J. W. Goodman, R. A. Dias, and L. M. Woody, Opt. Lett. **2**, 1 (1978).
[3] N. Farhat, D. Psaltis, A. Prata, and E. Paek, Appl. Opt. **24**, 1469 (1985).
[4] Y. Shi, D. Psaltis, A. Marrakchi, and A. R. Tanguay, Jr., Appl. Opt. **22**, 3665 (1983).
[5] A. Marrakchi, A. R. Tanguay, Jr., J. Yu, and D. Psaltis, Opt. Eng. **24**, 124 (1985).
[6] J. Yu, Ph.D. thesis, California Institute of Technology (1988).
[7] W. H. Steier, J. Kumar, and M. Ziari, Appl. Phys. Lett. **53**, 840 (1988).
[8] J. Hong, S. Campbell, and P. Yeh, in Proceedings of the SPIE Symposium on Spatial Light Modulators, San Diego, CA, Aug. 1989.
[9] A. M. Glass, Opt. Eng. **17**, 470 (1978).
[10] N. V. Kukhtarev, V. B. Markov, S. G. Odulov, M. S. Soskin, and V. L. Vinetskii, Ferroelectrics **22**, 949 (1979).
[11] T. J. Hall, R. Jaura, L. M. Connors, and P. D. Foote, Prog. Quantum Electron. **10**, 77 (1985).
[12] F. Vachss, Ph.D. thesis, Stanford University (1988).
[13] C. M. Bender and S. A. Orszag, *Advanced Mathematical Methods for Scientists and Engineers* (McGraw-Hill, New York, 1978).